

Neural adaptation in pSTS correlates with perceptual aftereffects to biological motion and with autistic traits

Steven M. Thurman^{a,*}, Jeroen J.A. van Boxtel^b, Martin M. Monti^a, Jeffrey N. Chiang^a, Hongjing Lu^{a,c,**}

^a Department of Psychology, University of California, Los Angeles 90095, USA

^b School of Psychological Sciences and Monash Institute of Cognitive and Clinical Neurosciences, Monash University, Clayton 3800, Vic, Australia

^c Department of Statistics, University of California, Los Angeles, 90095, USA

ARTICLE INFO

Article history:

Received 17 December 2015

Revised 22 March 2016

Accepted 4 May 2016

Available online 7 May 2016

Keywords:

Perceptual adaptation

Autism

Human actions

fMRI adaptation

Action aftereffects

ABSTRACT

The adaptive nature of biological motion perception has been documented in behavioral studies, with research showing that prolonged viewing of an action can bias judgments of subsequent actions towards the opposite of its attributes. However, the neural mechanisms underlying action adaptation aftereffects remain unknown. We examined adaptation-induced changes in brain responses to an ambiguous action after adapting to walking or running actions within two bilateral regions of interest: 1) human middle temporal area (hMT+), a lower-level motion-sensitive region of cortex, and 2) posterior superior temporal sulcus (pSTS), a higher-level action-selective area. We found a significant correlation between neural adaptation strength in right pSTS and perceptual aftereffects to biological motion measured behaviorally, but not in hMT+. The magnitude of neural adaptation in right pSTS was also strongly correlated with individual differences in the degree of autistic traits. Participants with more autistic traits exhibited less adaptation-induced modulations of brain responses in right pSTS and correspondingly weaker perceptual aftereffects. These results suggest a direct link between perceptual aftereffects and adaptation of neural populations in right pSTS after prolonged viewing of a biological motion stimulus, and highlight the potential importance of this brain region for understanding differences in social-cognitive processing along the autistic spectrum.

© 2016 Elsevier Inc. All rights reserved.

Introduction

A hallmark of the human visual system is its ability to recognize diverse actions by analyzing complex and hierarchical movements of the limbs of the body, termed biological motion perception (Johansson, 1973). Research has shown that prolonged viewing of an action (e.g., a walker) demonstrating a certain attribute (e.g., gender, walking direction, action category, 3D viewpoint) can bias judgments of subsequent actions towards the opposite of this attribute (Jackson and Blake, 2010; Troje et al., 2006; Theusner et al., 2011; van Boxtel and Lu, 2013a). Such experience-dependent plasticity allows the visual system to maintain high sensitivity to novel activities in a rapidly changing environment (Webster et al., 2005; Clifford et al., 2007). Because the social world is continuously in flux, it is important to remain sensitive to small changes in social cues. Hence, adaptation may be of extreme importance for stimuli such as biological motion that reveal social intentions and

guide inter-personal interactions. An inability to adapt may make one less able to detect social changes and respond to them appropriately.

However, the fundamental neural mechanisms underlying adaptation to biological motion remain unknown (Clifford et al., 2007). Investigating this issue is important for understanding short-term plasticity in the brain (Webster, 2011). In addition, individual differences in adaptability have potential implications for understanding limitations in social perception associated with Autism Spectrum Condition (ASC) (Pellicano et al., 2007; Pavlova, 2012). This last point is emphasized by recent findings indicating that individuals with ASC, and typically-developing individuals with many autistic traits, show reduced adaptation aftereffects for human faces (Pellicano et al., 2007) and biological motion (van Boxtel and Lu, 2013a), respectively.

A hurdle in studying action adaptation is that a vast network of brain areas is involved in processing biological motion information (Grossman et al., 2000; Grossman and Blake, 2002; Pelphrey et al., 2005; Saygin, 2007; Lestou et al., 2008). Human brain-imaging studies are thus required to pinpoint the contribution of neural adaptation in lower-level and higher-level processing regions to perceptual aftereffects for biological motion. We conducted a targeted functional magnetic resonance imaging (fMRI) experiment to measure neural adaptation within two functionally and anatomically distinct regions of interest: 1) the human middle temporal complex (hMT+), which

* Correspondence to: S.M. Thurman, UCLA Department of Psychology, 1282 Franz Hall, Los Angeles, CA 90095, USA.

** Correspondence to: H. Lu, Department of Statistics, University of California, Los Angeles 90095, USA.

E-mail addresses: sthurman@ucla.edu (S.M. Thurman), hongjing@ucla.edu (H. Lu).

has been linked to lower-level aspects of motion processing (Huk et al., 2002), and 2) the posterior superior temporal sulcus (pSTS), which has classically demonstrated strong selectivity for human actions and biological motion stimuli (Grossman et al., 2000).

Adaptation effects are typically measured in fMRI using repetition suppression: the brain response to repeated stimulation is reduced when compared to a novel stimulus that varies along some perceptual dimension. This technique can reveal the tuning properties of cortical regions at sub-voxel resolution (Grill-Spector and Malach, 2001; Krelberg et al., 2006; Webster et al., 2005). In terms of biological motion, Grossman et al. (2010) used the fMR-adaptation technique to show that neural populations in pSTS have action-specific tuning properties that are invariant to changes in viewpoint and retinal position. Although these results highlight the general importance of pSTS in biological motion perception and the capacity of this brain region to adapt to action specific information, it remains unclear to what extent the changes of brain activities in pSTS can account for changes and individual differences in perception (i.e. aftereffects) as a result of longer-term action adaptation. To fill this gap in knowledge, the present study aims to localize the neural correlates of aftereffects induced by adaptation to biological motion within areas of the motion and action processing systems. We also examine the relationship between neural adaptation to biological motion and the degree to which a typically developing individual adult has the traits associated with the autistic spectrum.

Materials and methods

Participants

A total of 12 healthy adult participants (mean age = 22.5 years, 7 female) enrolled and completed the study. Participants were recruited from the University of California, Los Angeles (UCLA) and gave written informed consent as approved by the UCLA Institutional Review Board. Participants received monetary compensation (\$30/h) for participating in the study. After an initial one-hour behavioral test session in the laboratory, fMRI scanning was completed across two separate days, typically lasting about 1.5 h each. All participants had normal or corrected-to-normal vision and had no reported neurological or visual disorders.

Participants completed the 50-point Autism-spectrum Questionnaire (AQ) to generate AQ scores, which provided an assessment of the degree to which individuals with normal intelligence have the traits associated with the autistic spectrum (Baron-Cohen et al., 2001). Because we aimed to measure individual differences in neural adaptation as a function of autistic traits, our sample population was selected using an extreme-group approach. We recruited typically-developing participants with either a relatively low AQ score ($n = 6$, mean = 12.5 ± 3.9) or a high AQ score ($n = 6$, mean = 28.3 ± 4.1). None of these subjects had participated in a prior behavioral adaptation study (van Boxtel and Lu, 2013a), and all were naïve to the purpose and design of the current study. Extreme-group designs are useful in fMRI work as they increase statistical power and cost efficiency (Preacher et al., 2005). Based on the recommendations of Preacher et al., in addition to the group comparison (based on dichotomizing subjects with different degrees of autistic traits according to their AQ scores), our analyses included statistical tests treating AQ as a continuous variable.

Stimuli and procedure

Point-light biological motion stimuli were generated from a free online motion-capture database (<http://mocap.cs.cmu.edu>), which has been used in previous research to study biological motion perception (van Boxtel and Lu, 2012; Thurman and Lu, 2013a, 2013b, 2014a, 2014b). Raw motion capture data were converted to point-light format using the Biomotion toolbox (van Boxtel and Lu, 2013b). We employed

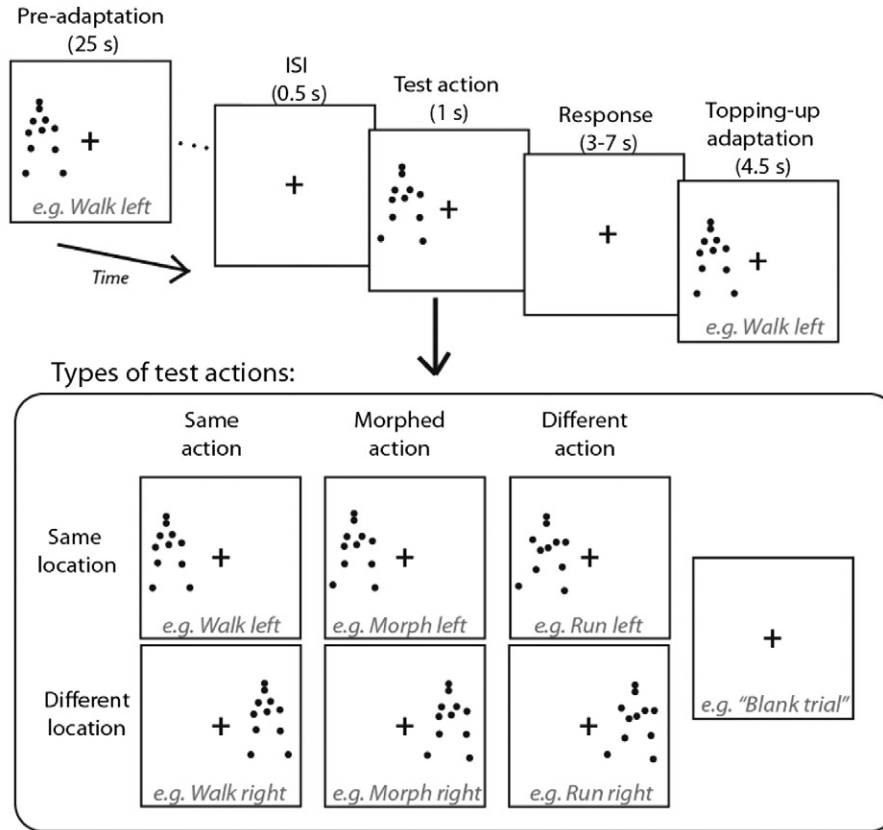
stimuli of adult humans walking and running, presented in the sagittal view and with the horizontal translation component removed such that the actor appeared to walk or run on a treadmill. Gait cycle length was equalized between the walker and runner stimuli (1.18 s). To produce stimuli systematically morphed between walking and running for the adaptation experiment, we used a morphing algorithm to generate ambiguous actions morphed between two prototypical actions (Giese and Poggio, 2000). For instance, in our experiment a morph weight of 0 indicates a stereotypical running action, a value of 0.5 generates an ambiguous action between running and walking, and a morph weight of 1 yields a stereotypical walking action. For all stimuli, facing direction was controlled by keeping it constant across subjects (always facing rightward for all subjects). In the experiment, point light actors (adaptors and test stimuli) subtended 4.9° vertically and individual dots had a diameter of 0.56° .

At the beginning of the experiment we measured an individualized level of morph weight for each participant that was then used for the subsequent behavioral and fMRI experiments. Participants were asked to identify the action (i.e., walking or running) after viewing a morphed stimulus. An adaptive staircase procedure adjusted the morph weight according to behavioral decisions (Prins and Kingdom, 2009) to estimate the threshold at which each subject could provide “running” responses with a proportion of approximately 35%. The adaptive staircase fitted a cumulative Gaussian function using the psi-marginal method over the course of 60 trials to produce an estimate of threshold for morph weight. The selection of 35% as the criterion was motivated by a prior study (van Boxtel and Lu, 2013a) to help distinguish random responses (which would yield 50% running responses) from no-adaptation responses (which would yield 35% running responses). Hence for a given subject, once the threshold of morph weight was determined, the same morph action was presented in subsequent experiments for that individual.

As illustrated schematically in Fig. 1a, each block of the main adaptation experiment began with a lengthy period of pre-adaptation (25 s) to the adapting stimulus. The adapting stimulus consisted of a point-light walker or runner shown with black dots. A red fixation mark (0.3° diameter) was located in the center of the gray screen, and adapting stimuli were presented with an offset of either 3.5° to the left or right of fixation. The pre-adaptation stimulus was followed by a blank inter-stimulus interval (0.5 s) and then a test point-light stimulus was presented with white dots (1 s) to help to distinguish it from the adapted stimulus. Test stimuli comprised a walker, a runner or a morph action presented with an offset of 3.5° to the left or right of fixation, either coinciding with the same location as the adapter or else presented in the opposite visual field. A variable period of passive fixation (3–7 s determined by an exponential distribution) followed each test stimulus, and participants were instructed to respond with a button press as to whether the test stimulus was perceived to be walking or running during this time window. The inter-stimulus-interval (ISI) was randomly jittered between 3 and 7 s because previous studies have shown that this procedure increases the efficiency for extracting event-related responses from fMRI BOLD signals (Dale, 1999; Serences, 2004), and reduces the predictability of the timing for the next trial. Following the fixation period was a period of topping-up adaptation (4.5 s), in which the designated adapting stimulus was again presented to reinforce the adaptation throughout the block of trials (Fang et al., 2007a; Fang et al., 2007b). After each period of topping-up adaptation, a blank inter-stimulus-interval (0.5 s) was followed by another test stimulus (1 s). Participants were directed to maintain fixation throughout the experiment.

Test stimuli were presented either in the same location as the adapting stimulus, or in a different location. The purpose of testing after-effects in a different location was to measure adaptation for position-invariant neural populations that represent the action characteristics at a global level (i.e. in a non-retinotopic manner) (Van Boxtel and Lu, 2013a). The six types of test stimuli were randomly intermixed with

a. Adaptation scans



b. No-adaptation (e.g. control) scans

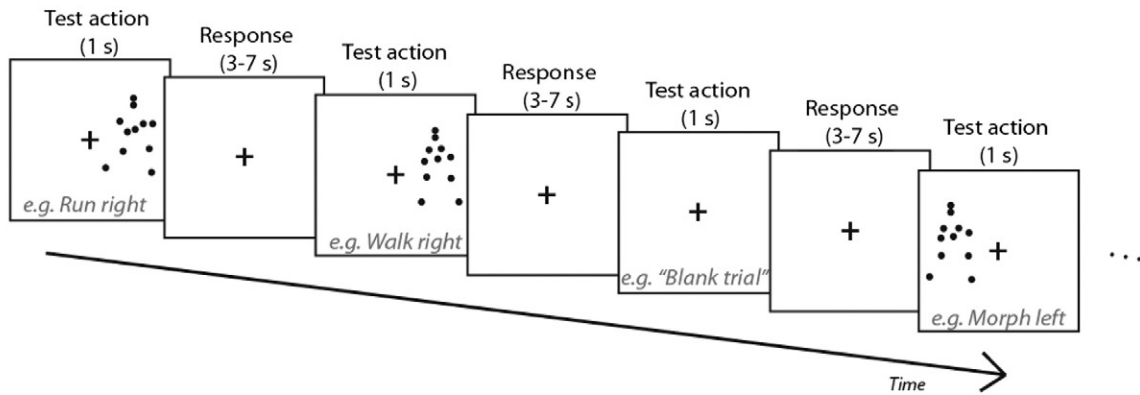


Fig. 1. Schematic of stimuli and design for (a) the behavioral adaptation experiment and fMRI adaptation scans, and (b) no-adaptation control scans in the fMRI experiment. Adapting actions varied per block and included runners or walkers shown on the left or right side of fixation (indicated by cross). Testing actions could be runners, walkers or morphs shown in the same or a different location. No-adaptation scans showed the same types of test actions, but without adaptation. Both scan types included “blank” fixation trials to compute percent signal change from baseline responses.

passive blank fixation trials (1 s) in a block of 56 trials, including a total of 8 trials per condition. Participants completed four blocks, each including adaptation to one stereotypical action (walker, runner) in one location (left, right). Block order was randomized for each participant. The fMRI experiment had the same design as the behavioral experiment, except participants completed 8 blocks total across two scanning sessions.

MRI acquisition

Neuroimaging data were collected on a 3 Tesla Siemens Tim Trio scanner (Siemens AG, Munich, Germany) located on the UCLA campus.

A high resolution T1-weighted (MP-RAGE) anatomical image of the whole brain (TR = 1900 ms, TE = 2.26 ms, FOV = 256|240|160 mm, FA = 9°, resolution 1 mm³ isovoxel) was collected from each subject at the beginning of each day of scanning for co-registration of the functional scans from that session. In each session, participants engaged in a total of seven functional scans (T2*-weighted gradient echo planar images, 33 interleaved slices, TR = 2000 ms, TE = 30 ms, 3 × 3 × 3.9 mm³, flip angle = 77°, with A to P phase encoding), including two localizer scans to identify specific functional regions of interest (ROIs), a control scan to measure the response to test action stimuli without the influence of perceptual adaption, and four experimental scans that included topping-up adaptation.

MRI procedure

Localizer scans

Localizer scans were used to identify functional regions of interest in the posterior superior temporal sulcus (pSTS) and middle temporal cortex (hMT+), as determined by their sensitivity to human action stimuli and moving dot stimuli, respectively. We used a standard pSTS localizer (Grossman et al., 2000, 2010), which contrasts neural responses to intact point-light biological motion with spatially-scrambled versions of the same point-light stimuli (Fig. 2b). While scrambled stimuli maintain the same local motion properties as intact stimuli, they typically do not result in the coherent perception of human activity due to the loss of global structural information. Point-light stimuli consisted of 25 unique actions (e.g., walking, squatting, throwing, jumping jack). This stimulus set has been used extensively in previous studies to localize action-sensitive regions in superior temporal cortex (Grossman et al., 2000, 2010; Pyles et al., 2007). Stimuli were presented centrally and

subtended 3.25° vertically. Using a blocked design, six blocks of intact biological motion were interleaved with six blocks of scrambled biological motion. Each block lasted 14 s and included 7 stimulus presentations, each lasting 1 s with an inter-stimulus-interval of 1 s. Between each block, we inserted a 6 s passive fixation period to allow the blood oxygenation level dependent (BOLD) signal to partially return to baseline. Participants were asked to maintain fixation throughout the 4-min scan and to press a button when any stimulus repeated (1-back task) to help maintain attention on the action stimuli.

To identify lower-level motion-sensitive regions, the hMT+ localizer included fields of optic flow (expanding and contracting dots of high contrast) presented alternately in the left and right hemifields (Huk et al., 2002). Optic flow was constrained within a circular region of radius 3.3°, offset by 5° from the center fixation point. Optic flow was presented in each hemifield for 14 s, followed by a fixation period with stationary dots for 14 s (Fig. 2a). Six repetitions were included in each scan. Throughout the 4:40 min scan, participants were instructed

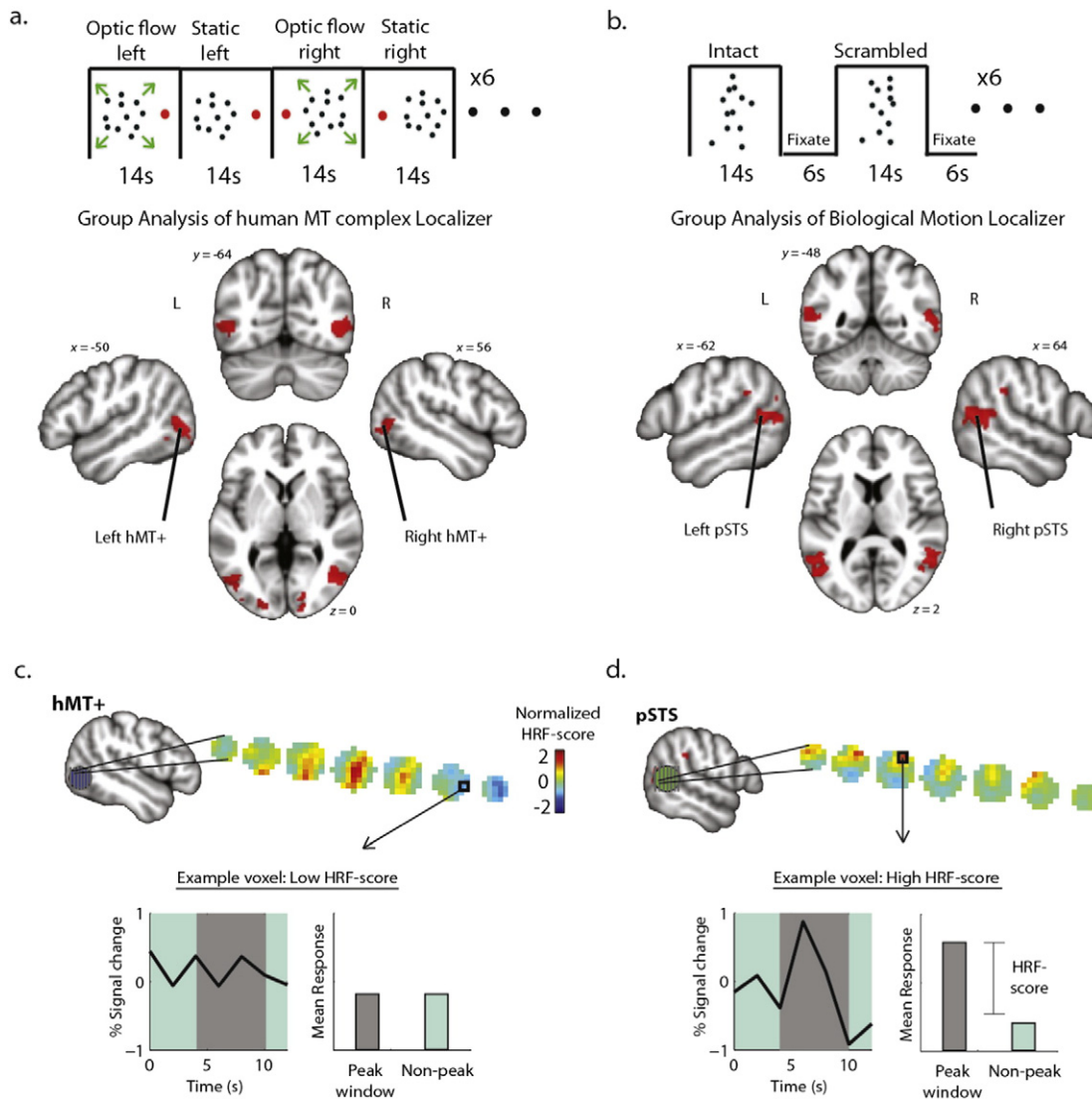


Fig. 2. Timeline of blocked-design localizer scans and group results of the general linear model for (a) the human medial temporal complex (hMT+; optic flow–static contrast), and (b) the posterior superior temporal sulcus (pSTS; biological–scrambled motion contrast). Thresholded activation maps are shown overlaid on a standard MNI brain template. Cluster-level threshold of activation map, $z = 2.3$, $p < 0.01$. (c,d) Depiction of the location of 8 mm spherical ROIs for hMT+ and pSTS on a standard brain (MNI template), and example data from a single subject showing 2d slices through each ROI in terms of HRF-score for each voxel. For visualization, HRF-scores were normalized (z-scored) across all voxels in each ROI, and roughly all voxels above the mean (z -score > 0 ; yellowish-red regions) were considered “signal” voxels in subsequent analyses. The lower plots illustrate BOLD responses for example voxels that happened to have a low HRF-score (c), or high HRF-score (d).

to maintain fixation and observe the moving dots. Each participant completed two scans for each localizer across two separate sessions.

Experimental scans

Experimental scans with adaptation employed a rapid event-related design in which test stimuli were interleaved with adapting stimuli. Experimental scans were designed to measure neural adaptation originating from changes in response to the morphed stimulus as a function of the different adapting stimuli, as well as to measure the change of brain responses when repeating identical actions versus viewing different actions (i.e., repetition suppression). The design of the experimental scan is described above and shown schematically in Fig. 1. In each session, participants completed four experimental scans (each lasting 7 min), adapting to each action (walker, runner) in each location (left, right) in pseudo-random order across the two sessions. Participants were trained and instructed to maintain fixation on the central fixation point for the duration of the experiment. The experiment included 2 adapting types (walker, runner), 2 locations (same, different) and 3 test action types (walker, runner, morph), and a total of 64 trials per condition, evenly distributed across all scans.

Control scans

Subjects participated in the control scans in order to measure the neutral brain response to the point-light actions used in the experiment (walker, runner and morph presented in the left or right hemifield), without the influence of adapting stimuli. Control scans used a rapid event-related design (Fig. 1b) to estimate a baseline response for each ROI to each of the action stimuli, and to determine whether any of the ROIs had an inherent bias in the response to one action type over another. Point-light actions were presented with white dots (0.56° diameter) on a gray background for 1 s, followed by a variable inter-stimulus-interval (ISI) between 3 and 7 s determined by an exponential distribution. Biological motion stimuli were also randomly intermixed with blank trials of 1 s passive fixation in order to acquire a baseline response for computing percent signal change. Participants indicated with a response box as to whether the stimulus was perceived to be walking or running during the fixation period following each test stimulus. Each scan lasted approximately 4:40 min, with 8 repetitions of each of the 7 trial types. Participants completed 2 control scans across two separate sessions.

Data processing and analysis

Preprocessing was conducted with FSL (Smith et al., 2004), and the extracted BOLD timecourses were analyzed with Matlab (Mathworks). The first five volumes of each scan were removed to allow saturation of the MR signal. We used FSL's built-in brain extraction tool (BET) to isolate neural tissue from other tissues (e.g., skull) prior to preprocessing. All functional brain images were corrected for head movement within each scan, and then co-registered (6 dof) with the high-resolution anatomical scan to align all functional scans within each session by using FSL's linear registration tool (FLIRT) (Jenkinson and Smith, 2001; Jenkinson et al., 2002). High-pass filtering (0.01 Hz) removed linear drift from the BOLD signal. Spatial smoothing (5 mm) was applied to the localizer scans, but no smoothing was applied to the experimental or control scans. Participant's scans were normalized by warping the high-resolution anatomical scan (12 dof) to fit the Montreal Neurological Institute (MNI) standard template (avg152 T1-weighted template, 1-mm isovoxel) to facilitate statistical analysis in a common brain space for data collected across different scan days and across individual subjects. Brain images from functional scans were re-sampled to 1-mm isovoxel resolution to match the resolution of the standard template.

Analysis for localizer scans

Localizer scans were analyzed with a general linear model. Predictors were estimated with a boxcar function representing each block of

stimulation convolved with a model of the hemodynamic response function (HRF) (Boynton et al., 1996). Action-sensitive regions were estimated by contrasting beta estimates from biological motion blocks minus scrambled blocks. Motion sensitive regions in right hemisphere cortex were estimated by contrasting left hemifield optic flow with left stationary dots, and regions in the left hemisphere were estimated by contrasting right hemifield optic flow with the block of right stationary dots. We applied cluster-level thresholding in FSL (z -score = 2.3, $p < 0.01$) to identify significant regions of activation for each participant. Using the statistical maps and anatomical criteria, we identified the voxel with peak activation within the left and right pSTS from the biological motion localizer scans, and within left and right middle temporal cortex from the optic flow scans. This voxel served as the center of a spherical volume (8 mm diameter for a total of 257 voxels at 1-mm isovoxel resolution), which represented the region of interest in standard space individually for each subject. The fixed-size ROI volume was used to equate the total number of voxels contributing to multi-voxel pattern analysis across subjects and across distinct cortical regions. To increase signal-to-noise, subsets of voxels were later selected according to action selectivity (see Materials and methods: Voxel selection). We were able to successfully identify pSTS and hMT+ bilaterally in each subject (Table 1). To show group-level activation maps across subjects, a mixed-effects group analysis was performed and the results for each functional localizer are displayed in Fig. 2.

N indicates the number of subjects for which we were able to identify a given ROI, out of the total number of subjects. X, Y, and Z represent the mean MNI coordinates for each isolated ROI across subjects using the independent functional localizer scans described in the text. ROI names: posterior superior temporal sulcus (pSTS) and human middle temporal area complex (hMT+).

Analysis for control scans

To analyze event-related responses for control scans, BOLD timecourses were extracted from voxels specified by each ROI and imported into Matlab (Mathworks). As the first step in analysis, we proceeded voxel-by-voxel in the 8 mm spherical ROI to compute event-related responses for each type of test action in the control scans. Event-related responses were computed by selectively averaging the BOLD signal to events within a 12 s window time-locked to the onset of the test stimulus, following the methods of previous studies (Dale and Buckner, 1997; Kourtzi and Kanwisher, 2000; Fang et al., 2007a). The average intensity of BOLD signal during fixation trials was used as a baseline to convert event-related signals to percent signal change by subtracting the corresponding value from the fixation response and dividing by that value.

Voxel selection

Inspecting the event-related responses voxel-by-voxel in the control scan, it was apparent that while many voxels contained responses resembling a canonical hemodynamic response function (HRF), some other voxels appeared to have either no inherent signal or large amounts of noise. In addition, while the 8 mm sphere was centered on the peak cortical activation for each ROI, this rather large volume may

Table 1
Mean MNI coordinates for ROIs isolated independently for each subject.

ROI	N	X	Y	Z
<i>Right hemisphere</i>				
pSTS	12/12	55.8	−51.7	11.0
hMT+	12/12	48.7	−65.7	4.0
<i>Left hemisphere</i>				
pSTS	12/12	−54.3	−52.7	11.7
hMT+	12/12	−48.2	−70.8	3.5

nonetheless have included nearby white matter or cortical voxels with limited sensitivity to biological motion. To remove the influence of such noisy voxels from the ROI-based analysis, we used the data in the control scan to focus on a selected set of voxels for targeted analysis in the experimental scans. Analysis using the selected subset of voxels did not change the results qualitatively relative to an analysis without the selection process, but effectively increased the signal-to-noise ratio for comparing adaptation effects across different conditions. We developed two methods to select relevant voxels, one based on an unbiased and agnostic measurement of how well the mean event-related response to stimulation resembled a typical hemodynamic response, and another based on the voxel discriminability of classifying walking and running actions using multi-voxel pattern analysis (MVPA).

In the first method, we computed a measure termed HRF-score for each voxel in a given ROI, reflecting the degree to which the mean response across all action types in the control scan roughly resembled a canonical HRF (Fig. 2c,d). An HRF-score was computed by subtracting the average response in the presumed peak window of activation (from 4 to 10 s) from the average response in time points outside this peak window (0, 2, and 12 s). We used the mean response across all 6 test conditions (walk, run, morph presented in the left and right hemifields) to ensure that the estimate was not biased to any particular action or location. A high HRF-score indicates a good resemblance to a canonical HRF because it reflects an increased BOLD response between 4 and 10 s post-stimulus relative to the onset and offset of the hemodynamic response (Boynton et al., 1996). Voxels with a noisy response would yield a low HRF-score due to a lack of characteristic response to action stimuli.

By examining the consistency of HRF-scores across voxels, we observed reliable clustering of high-score voxels across the 8 mm spherical volume and across control scans for each subject (Fig. 2c,d). On this basis, we selected the top 50th percentile of voxels (128 voxels for each of the 4 ROIs including left and right hemisphere hMT+ and pSTS) for use in the targeted analysis for the experimental scans. It must be emphasized that voxel selection was based on the brain responses to all test actions in the control scans, and hence was independent from brain activities measured during the experimental scans where adaptation took place. This selection procedure avoids the problem of circularity in our data analysis (Kriegeskorte et al., 2009). Also, when the analysis was repeated with a range of criteria (top 10, 30, 50, 70, 90% of voxels) the results were qualitatively unchanged.

In the second method, we used support vector machine based searchlight MVPA to identify subpopulations of voxels within the ROIs that could discriminate walking versus running. The features for the classifier were a “beta-series” of single trial parameter estimates (Rissman et al., 2004), which were constructed using the Least-Squares-Separate method described by Mumford et al. (2012). Using a 2 voxel (4 mm) radius searchlight, we tested the local performance of small clusters of voxels within each ROI in a 10-fold cross validation procedure (i.e. train the classifier on 90% of the trials, and test on the remaining 10%). The searchlight analysis was carried out in MATLAB, with the searchlight framework based on the RSA toolbox (Nili et al., 2014), and SVM implemented by LibSVM (Chang and Lin, 2011). On the basis of classification accuracy, we chose the top 20% of voxels (mean = 57 voxels \pm 10.6) in each ROI that reached above chance (>50%) accuracy. The mean classification accuracy of the selected voxels across all subject ROIs was 55.2% (\pm 3.4), 59.2% (\pm 4.6), 58.4% (\pm 3.7), and 58.4% (\pm 4.9) for the left hMT+, right hMT+, left pSTS and right pSTS, respectively.

In summary, the two proposed methods of voxel selection are distinct but can be viewed as complementary. In the case of HRF-score, voxel selection is less stringent and agnostic to the specific type of action presented, the degree of action selectivity, and the precise shape of the brain response, although the response must roughly match the presumed timecourse of the rise and fall of the HRF. In the case of MVPA-based selection, voxels are chosen specifically because they showed

differential responses to walkers versus runners to support discrimination with the statistical model.

Baseline action preference

Another important result revealed in the analysis of the control scans was the variations across participants, and across their ROIs, in terms of whether walking actions or running actions tended to evoke greater baseline brain activity on average. The proportion of participants showing greater brain response to walking compared to running action varied by ROI, with 4/12 participants showing a preference for walker in left hMT+, 5/12 in right hMT+, 7/12 in left pSTS, and 6/12 in right pSTS. A plausible explanation for such variability is that individual brain areas may include an uneven number of neurons selectively tuned to different actions, or their particular features, within a given region of cortex. For each ROI for each participant, we measured the proportion of the total number of voxels showing a preference for one action type or the other. If action preference were accidental or purely random, we would expect approximately half of the voxels to prefer one action and half the other. Based on this proportion, we performed a sign test to assess the statistical significance of voxel preference for each ROI. We found that 27 of 48 ROIs (consisting of 4 ROIs for each of 12 participants) showed a significant action preference, with a majority of voxels yielding greater brain activity for the walking action than for running. These inherent variations should be taken into account when estimating neural adaptation from the BOLD signal in the experimental trials. To measure the BOLD signal changes induced by the specific adapting action per se, we will use an absolute (i.e., non-relative) measure of the brain's response to a morph action and examine how the response is modulated by different adapting stimuli. In line with neurophysiological approaches, we will call the action that evokes the larger baseline response within the ROI the *preferred* action, and the action that evokes the smaller baseline response the *non-preferred* action.

Quantifying measures of neural adaptation in fMRI in experimental scans

To analyze data in experimental scans, we first extracted the mean BOLD timecourse from selected voxels in each ROI and used event-related averaging to estimate the brain response for each test condition. We computed two distinct measures of neural adaptation for each ROI. The first measure is a direct analog of the perceptual aftereffect, which we therefore call the neural aftereffect. This measure was designed to examine BOLD signal changes when a morphed action stimulus was presented after adapting to a preferred action versus after adapting to a non-preferred action. Behaviorally, participants are more likely to identify the ambiguous morph action as walking after adapting to a runner, and vice versa, signaling a reversal in perception (see Behavioral results in Fig. 3). Hence, perceptual aftereffects measured behaviorally are quantified by this difference in response proportions for judging the morphed action after adapting to one stereotypical action compared to responses after adapting to the other. In a similar manner, the measure of neural aftereffect strength was quantified as the peak response in a time window of 6–10 s post-stimulus-onset for morph actions after adapting to the non-preferred action minus the peak response after adapting to the preferred action. Note that after adapting to a preferred action the subsequently presented morph will be more likely to be perceived as the non-preferred action, and thus the ROI should show a decreased activity in comparison to when the non-preferred action was adapted. To show neural aftereffects consistent with the directionality of perceptual aftereffects measured behaviorally, we expected an increase of the brain response to the morph action after adapting to the non-preferred action (e.g. runner-adaptor in the above example). Likewise, we expected a decrease of the brain response to the morph action after adapting to the preferred action (e.g., walker-adaptor in the example). This procedure allowed us to assess not just the magnitude of neural adaptation to the morph (e.g. the absolute difference in morphed responses as a function of the type of adapting action), but

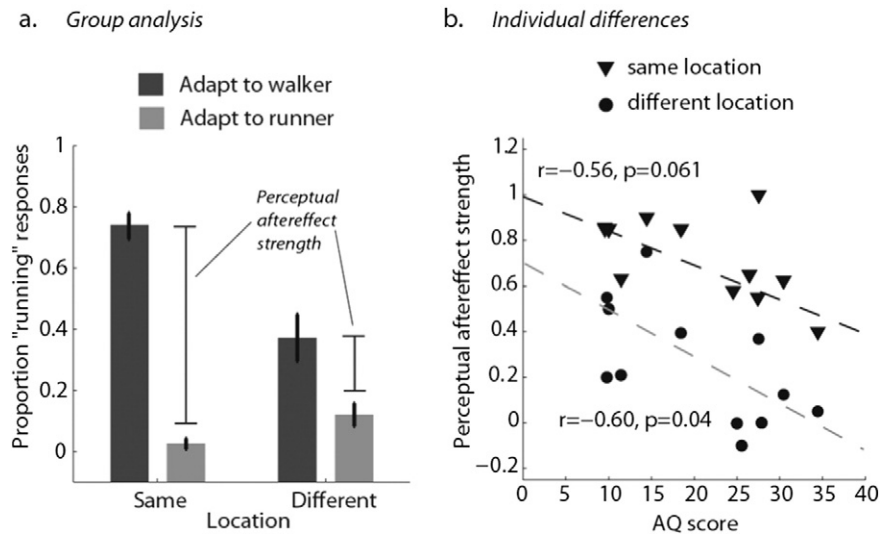


Fig. 3. Results of the behavioral experiment completed prior to fMRI scanning, showing (a) perceptual aftereffects for morphed actions presented in the same or in different location as compared to the adapting action, and (b) a significant correlation across individual subjects between perceptual aftereffect strength and the degree of autistic traits (measured by AQ score). Perceptual aftereffect strength was quantified by subtracting the proportion of running responses on the morphed action after adapting to walker versus runner (walker–runner).

also its directionality. If we found that the adaptation-induced difference in response to the morph was opposite to the above scenario, then this would indicate a priming effect because the change in response would be in the same direction as the inherent response preference of the ROI.

The second measure of neural adaptation is fMR-adaptation index, revealed by decreased brain responses to repeated stimulation, which is closely related to repetition suppression and has been used extensively as a paradigm to study the selectivity of neural populations in human visual cortex (Grill-Spector and Malach, 2001; Kourtzi et al., 2003; Weiner et al., 2010). In the analysis of adaptation resulting from repetition suppression, we focused on the walking and running test stimuli, and examined the difference between repeated actions (e.g., adapt walker, test walker) and categorically distinct actions (e.g., adapt walker, test runner). Hence, while the measure of neural aftereffects estimated adaptation-induced change in response to ambiguous morphed stimuli, the measure of fMR-adaptation estimated the more generalized effect of repetition suppression focusing on stereotypical actions. Specifically, in this analysis, we first transcoded the trial labels for each condition into four categories as follows: 1) repeated stimulus (i.e., adapting and testing stimuli are the same, such as adapt walker, test walker; or adapt runner, test runner) in the same location, 2) repeated stimulus in a different location, 3) different stimulus (i.e., adapting and testing stimuli are different, such as adapt walker, test runner; adapt runner, test walker) in the same location, and 4) different stimulus in a different location. In each condition, the fMR-adaptation index was computed by subtracting the peak response within a window of 6–10 s post-stimulus-onset for repeated actions from different actions (different–repeated). A typical fMR-adaptation effect due to repetition suppression would be represented by a reduced response to repeated stimulation; hence positive index values would indicate stronger repetition suppression effects (Pyles et al., 2007; Grossman et al., 2010).

Results

Behavioral results

For each condition in the initial behavioral study (completed prior to brain scanning), we computed the proportion of trials in which the subject reported a “running” action when presented with a morph action (Fig. 3a). Participants showed significant perceptual aftereffects to

biological motion, as indicated by the fact that they were more likely to identify a morph action as “running” after adapting to a walker, and less likely after adapting to a runner. A 2×2 repeated-measures analysis of variance (ANOVA) revealed significant main effects of the adapting stimulus type (walker vs. runner), $F(1,11) = 74.9$, $p < 0.001$, and adapting location (same, different), $F(1,11) = 17.4$, $p = 0.002$. There was also a significant interaction between stimulus type and location, $F(1,11) = 56.9$, $p < 0.001$. The difference in the proportion of running responses between adapter types can serve as a measure of perceptual aftereffect strength. The interaction effect was due to significantly stronger aftereffects for morphed actions presented in the same location (mean = 0.71, ± 0.17) versus a different location (mean = 0.25, ± 0.26), $t(11) = 7.5$, $p < 0.001$, which is consistent with prior results (Van Boxtel and Lu, 2013a).

Further analysis revealed that perceptual aftereffects were negatively correlated with individual differences in terms of the degree of autistic traits as measured by AQ scores when adapting and test stimuli were presented in different locations, $r(11) = -0.60$, $p = 0.039$, and nearly significant when the two stimuli were presented in the same location, $r(11) = -0.56$, $p = 0.061$ (Fig. 3b). Again, consistent with prior results using a similar adaptation paradigm (Van Boxtel and Lu, 2013a), we found that participants with higher AQ scores (i.e., more autistic traits) showed a general reduction in the strength of perceptual aftereffects to biological motion, particularly for test stimuli presented in a different retinal location.

Neural aftereffect results

Neural aftereffects quantified the change and directionality of brain responses to ambiguous morph actions induced by different adapting stimuli. In this section, we first present analysis results of using selected voxels from the HRF-score method. Fig. 4 depicts mean event-related hemodynamic responses to morph actions in different conditions and the derived neural aftereffects within each ROI. In the motion selective area hMT+, significant neural aftereffect was revealed when adapting and testing stimuli were presented in the same location in the left hMT+, $t(11) = 2.5$, $p = 0.03$, but not for the different location conditions, $t(11) = 1.5$, $p = 0.160$, nor was it significant for any condition in the right hMT+ (both p 's > 0.25). These results indicate that neural populations within low-level motion-sensitive cortex (specifically, the left hemisphere hMT+) show location-specific adaptation for biological

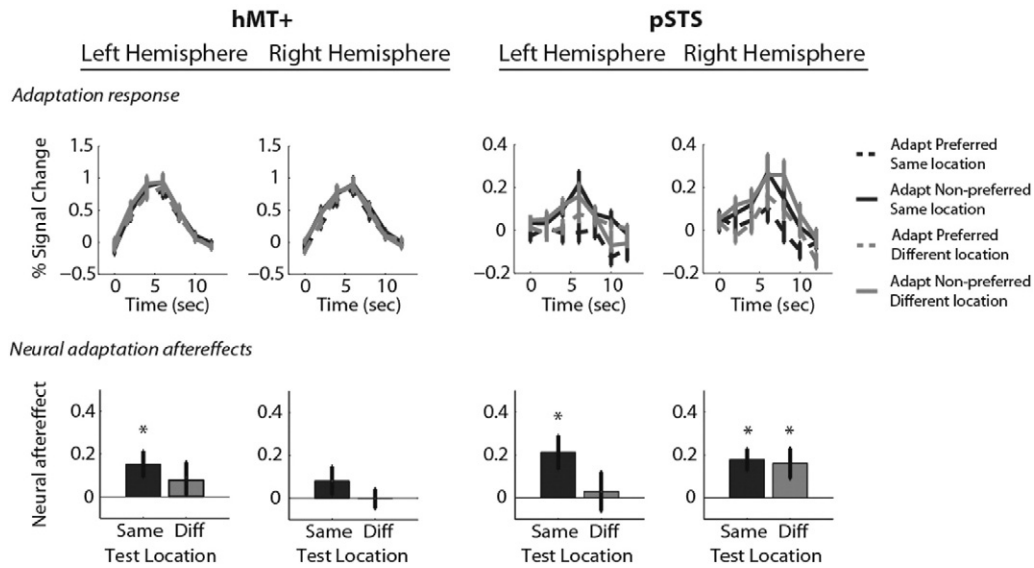


Fig. 4. Results of group-analysis for neural aftereffects in each hemisphere and ROI. Mean event-related hemodynamic responses to preferred and non-preferred actions in the control scans (top), mean event-related responses to morphed actions in the experimental scans depending on the specific adapting stimulus type (middle), and bar graphs showing the group mean of neural aftereffect strength (bottom). Positive values of neural aftereffect indicate neural responses consistent with the directionality of adaptation aftereffects derived from behavioral measures. Error bars represent SEM. * $p < 0.05$.

motion stimuli, but hMT+ in neither hemisphere shows location-invariant effects.

In comparison, significant neural aftereffects within the right pSTS were found for both the same location condition, $t(11) = 3.49$, $p = 0.005$, and the different location conditions, $t(11) = 2.26$, $p = 0.045$. For the left pSTS, neural aftereffect was significant for the same location condition, $t(11) = 2.7$, $p = 0.021$, but was not significant for the different location conditions, $t(11) = 0.33$, $p = 0.750$. The neural aftereffect of the left pSTS in the same location was greater than the effect in the different locations ($t(11) = 2.30$, $p = 0.031$). This difference may be due to the additive adaptation effect propagated from left MT and the relatively weak adaptation effect in the left pSTS in the same location condition. Hence, the right pSTS was the only region that showed significant adaptation-induced change of brain responses to morph actions regardless of location.

We examined the relationship between neural aftereffects measured from BOLD signal in each ROI, and behavioral measures of perceptual aftereffects across participants. Neural aftereffects were significantly correlated with perceptual aftereffects within the right pSTS in both the same location condition, $r(11) = 0.65$, $p = 0.024$,

and different location conditions, $r(11) = 0.66$, $p = 0.020$ (Fig. 5a). The left pSTS also showed a positive correlation between neural aftereffects with perceptual aftereffects in the same location condition that was not statistically significant, $r(11) = 0.47$, $p = 0.120$. None of the other correlations were significant for any other ROI or condition (all other p 's > 0.25). Note that due to technical failure of the button-recording apparatus in the scanner, we only measured perceptual aftereffect strength from the behavioral experiment collected prior to the fMRI scan sessions. On average, participants performed the behavioral session to measure perceptual aftereffects about 50 days prior to the fMRI scan sessions that measured neural aftereffects. Nonetheless, we found a strong positive correlation between fMRI measurements of neural aftereffects in right pSTS and individual performance in terms of perceptual aftereffects, demonstrating a relatively stable link between adaptability of neural populations within the right pSTS and behavioral performance in adaptation to biological motion.

We next examined the relationship between neural aftereffects derived from brain activities and individual differences in the degree of autistic traits. We found that participants with more autistic traits (i.e., high AQ scores) showed less neural adaptation in the action-

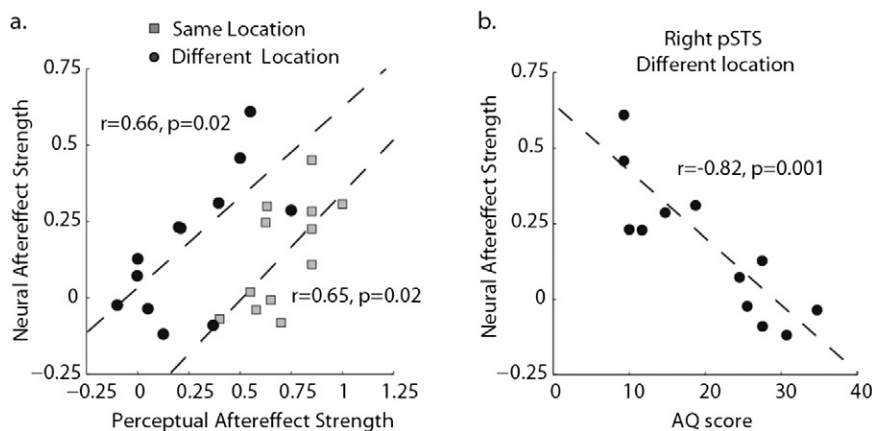


Fig. 5. Results of neural aftereffects in right pSTS in relation to perceptual aftereffects measured behaviorally, and to individual differences in the degree of autistic traits. (a) Scatter plot showing the significant correlation between perceptual aftereffect strength and neural aftereffect strength within the right pSTS. (b) Scatter plot showing the significant negative correlation between AQ score and neural aftereffect strength at the global level (i.e., adapt and test stimuli presented in different locations).

sensitive brain region, revealed by a strong negative correlation between AQ score and neural aftereffects in the right pSTS when morphed actions were presented in a different location from the adapting actions, $r(11) = -0.82, p = 0.001$ (Fig. 5b). This result was confirmed with a two-sample *t*-test between the low and high AQ groups, defined by a median split ($n = 6$ in each group), $t(7.3) = 4.36, p = 0.003$. We also found a nearly significant negative correlation between AQ score and neural aftereffects in the left pSTS when the adapt and test stimuli were presented in the same location, $r(11) = -0.57, p = 0.053$. AQ score was not correlated with neural aftereffects in area hMT+ for any condition (all other p 's > 0.243). These findings suggest an important link between the autistic traits of an individual and the adaptability of action-coding neural populations within the pSTS brain region.

Multi-voxel pattern analysis (MVPA) results

We repeated the same analysis to compute neural aftereffects, but used MVPA classification accuracy as an alternative criterion for selecting voxels (see [Materials and methods](#)). Overall, the results were quantitatively similar to those obtained from using the HRF-score method. For instance, the correlation between the strength of neural aftereffects and behavioral aftereffects was significant in the right pSTS for test stimuli in a different location, $r(11) = 0.69, p = 0.013$, and was close to the significance level for the same location, $r(11) = 0.57, p = 0.051$. This analysis also revealed a reliable correlation between neural aftereffects and the degree of autistic traits in the right pSTS for test stimuli in a different location, $r(11) = -0.80, p = 0.002$, consistent with the results reported above. Interestingly, the MVPA-based analysis also revealed a significant correlation between these factors within the right pSTS for test stimuli in the same location, $r(11) = -0.62, p = 0.001$, whereas this correlation showed a trending result (but was non-significant) using HRF-score as the voxel selection method, $r(11) = -0.37, p = 0.241$. This result suggests that MVPA-based voxel selection may be targeting more specialized neural populations to effectively increase signal-to-noise ratio in the measurement of neural adaptation effects. In fact, we found that about 50% of voxels on average were commonly shared between the two independent methods of voxel selection (left hMT+: 51%, $\pm 13\%$; right hMT+: 54%, $\pm 11\%$; left pSTS: 43%, $\pm 12\%$; right pSTS: 52%, $\pm 9\%$), indicating that they targeted relatively distinct neural populations with only moderate overlap.

We performed another set of analyses using MVPA methods to complement the aforementioned results on neural adaptation aftereffects. Using the MVPA-selected voxels, a classification analysis was run on the morph trials following adaptation to examine whether the influence of adaptation was reflected in neural activation patterns. A linear SVM classifier algorithm was applied to the beta-series to discriminate whether subjects had adapted to walkers or runners. The morph trials were selected because the stimuli were identical and yet perception would typically change according to the adapted action category. As such, differences in voxel activity should reflect altered perception rather than factors related to low-level stimulus features. A 10-fold cross-validation procedure was run in each ROI on the 128 morph trials (i.e. train on 90% of trials, and test on the remaining 10%). The labels were shuffled within runs 1000 times (a stratified permutation procedure) to generate a null distribution for classification accuracy.

The linear SVM was able to discriminate the action category of the adapter (walker vs. runner) preceding the morphed stimuli in all ROIs (left hMT+: 69.5%, $\pm 5.3\%$; right hMT+: 64.4%, $\pm 7.2\%$; left pSTS: 67.4%, $\pm 6.4\%$; right pSTS: 64.8%, $\pm 4.1\%$). Classification accuracies for all ROIs fell within the top 5% of values in the empirical distributions generated by the stratified permutation procedure (the top 5% cutoff was approximately 58% for all ROIs). Importantly, mirroring the results from the measure of neural aftereffects, we found that MVPA classification accuracy in right pSTS was significantly correlated with AQ score, $r(11) = -0.80, p = 0.002$, whereas the correlation in each other ROI was non-significant (all other p 's > 0.29).

Taken together, each method of analysis converged on the same main result indicating a strong relationship between changes in neural activity in the right pSTS brain region, the susceptibility of an individual to perceptual action adaptation aftereffects, and their intrinsic degree of autistic traits.

fMR-adaptation results

We examined repetition suppression, or fMR-adaptation (Pyles et al., 2007; Lestou et al., 2008; Grossman et al., 2010), by measuring the reduction in response for repeated actions as compared to different actions within each ROI. Results of this analysis are presented in Fig. 6. We found a significant fMR-adaptation originated from repetition suppression within the right pSTS when adapting and testing stimuli presented in the same location, $t(11) = 2.41, p = 0.035$, and a nearly significant effect of negative adaptation (i.e. priming) when presented in a different location, $t(11) = -2.15, p = 0.060$. There was no evidence for fMR-adaptation in bilateral hMT+ or in the left pSTS (all p 's > 0.10), which contrasts with previous findings (Grossman et al., 2010). We will discuss this discrepant result in the [Discussion](#) section.

To determine the extent to which repetition suppression induced fMR-adaptation could potentially explain behavioral performance in perceptual aftereffects, we evaluated the correlation between fMR-adaptation index and perceptual aftereffects across subjects. None of the correlation coefficients were significant (all p 's > 0.24), demonstrating that fMR-adaptation is a relatively weak predictor for perceptual aftereffects measured behaviorally. fMR-adaptation also did not show any significant correlations with AQ score for any ROI or location condition (all p 's > 0.33). These null results were also replicated in using MVPA as the basis for voxel selection. In comparison to the aforementioned measure of neural aftereffects for ambiguous morph action, which showed a strong correlation to behavioral data in the right pSTS, the general propensity for neural populations to decrease activity after stimulus repetition (i.e., fMR-adaptation) does not appear to be directly related to the phenomenon of perceptual adaptation.

Discussion

The brain constantly adapts (and desensitizes) to the prevailing input in order to remain sensitive to changes in the environment. In the current study, we examined this adaptation process by using a topping-up adaptation paradigm to measure behavioral and neural aftereffects to human actions represented as point-light biological motion. We measured perceptual adaptation aftereffects in typically developing subjects with varied degree of autistic traits, and related these behavioral differences to neural adaptation as measured by changes in brain responses using fMRI.

In order to investigate neural aftereffects, we devised a neural adaptation measure based on the same principles as the measure for perceptual aftereffects commonly used in behavioral experiments. Neural aftereffect strength was computed from the difference in response to identical morphed actions as a function of the preceding adapting action, taking into account the directionality of this difference by considering inherent differences in the baseline sensitivity of voxels within each ROI to the action category of the adapted stimulus. We found significant strength of neural adaptability within the action-selective area, the right pSTS, and this effect was location-invariant. This location-invariant characteristic was unique to the right pSTS across all ROIs studied, and therefore implicates the right pSTS as a primal region within the action processing system to account for action adaptation effects. Previous investigations have identified pSTS as a major hub in the brain network for recognizing biological motion (Grossman et al., 2000; Blake and Shiffrar, 2007; Saygin, 2007), and our results are in line with these findings. However, importantly, the present study links this area to action adaptation, an important functional aspect of perceptual plasticity.

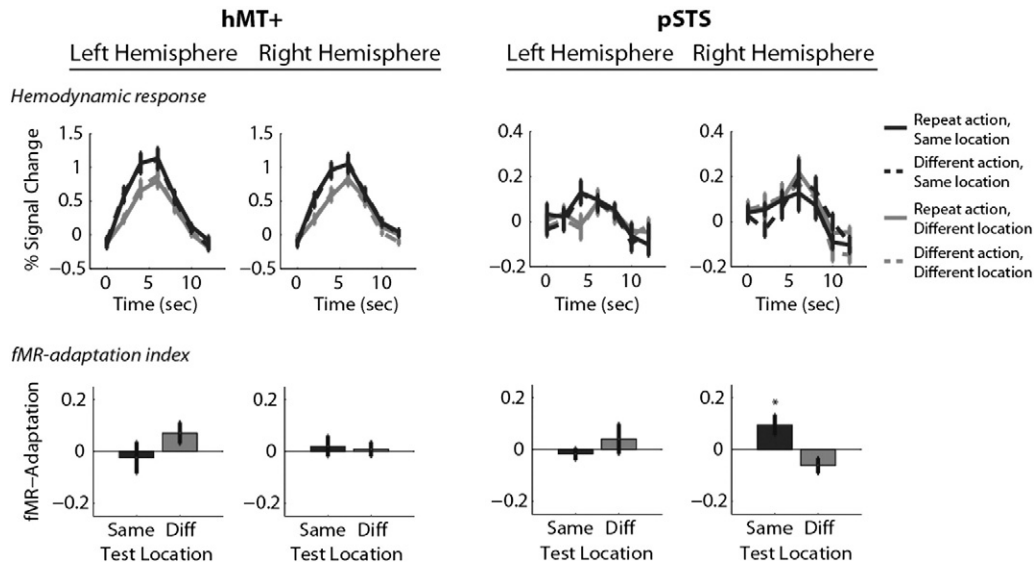


Fig. 6. Results of group-analysis for the measure of fMRI-adaptation (e.g. repetition suppression) in each hemisphere and ROI. Mean event-related hemodynamic responses to walking and running actions as a function of the location and type of adapting stimulus (top), and fMRI-adaptation index measures (bottom). Positive values of fMRI-adaptation indicate repetition suppression effects. The only significant effect of repetition suppression was found in right hemisphere pSTS for repeated actions presented in the same location ($*p < 0.05$). Error bars represent SEM.

Similar to the present findings, many previous studies have noted a hemispheric asymmetry related to biological motion processing in the pSTS region. Brain imaging studies have consistently reported stronger and more robust effects in the right hemisphere pSTS as compared to the left for biological motion (Grossman et al., 2000; Peuskens et al., 2005; Michels et al., 2009; Thompson and Baccus, 2011), and also for other types of stimuli such as human faces (Narumoto et al., 2001) and complex social stimuli (Castelli et al., 2000; Gallagher et al., 2000; Pelphrey et al., 2004). In our study, we found that the right pSTS is specifically involved in location-invariant aftereffects at a more global level, whereas the left pSTS is predominantly involved in location-specific aftereffects. These results are consistent with the hypothesis that the right hemisphere pSTS plays a specialized role in biological motion and social processing (Allison et al., 2000).

An essential part of our study was to acquire behavioral measures of perceptual adaptation to biological motion (van Boxtel and Lu, 2013a), and to relate behavioral performance to brain activity. We found that the degree of neural adaptation measured from the right pSTS was a significant predictor of perceptual aftereffects derived from behavioral responses. We further show that the strength of neural aftereffects in the right pSTS was also significantly correlated with individual differences in terms of autistic traits. These results were replicated using MVPA classification accuracy as an alternative criterion to select relevant voxels in the ROI volume, and were further corroborated using a complementary measure of neural adaptation derived from MVPA classification accuracy. In each case we found converging evidence for a specific and significant relationship between fMRI measurements and both behavioral adaptation and autistic traits.

As noted earlier, the sample size used in the present study is consistent with those used in previous studies examining perceptual adaptation effects in fMRI (e.g., Fang et al., 2007a; Zhang et al., 2014). Importantly, each participant in our study was scanned for three hours in order to collect extensive and reliable data reflecting the influence of adaptation on subsequent percepts, on a trial-by-trial basis. In addition to a correlation analysis, we conducted a group comparison by contrasting performance of participants with less autistic traits to that of participants with more autistic traits, and examined MVPA classification accuracy using multivariate analyses. These three different methods of analysis converged on the same key finding: a strong relationship between adaptation-induced

changes in neural activity in the right pSTS brain region, and individual differences based on the degree of autistic traits.

Prior studies have documented differences between individuals with ASC and typically-developing populations in terms of brain activation within the pSTS during biological motion processing (Herrington et al., 2007; Freitag et al., 2008; Kaiser and Pelphrey, 2012; McKay et al., 2012), suggesting that deficits in biological motion perception may represent a hallmark condition of ASC (Pavlova, 2012). Our results extend the scope of this research line by showing that the perceived attributes of human movements after prolonged viewing of an action can vary from person to person, and that much of this variation can be explained by the adaptability of neural populations within pSTS and the degree of autistic traits in typical-developing individuals.

Research on the impact of autism on biological motion perception has yielded mixed results (Cusack et al., 2015; Freitag et al., 2008; Klin et al., 2009; Murphy et al., 2009; Saygin et al., 2010; McAleer et al., 2011). One primary factor that has led to mixed results regarding the relation between autism and biological motion perception is that different studies have probed different levels of hierarchical processing for biological motion perception (local processes specialized for detecting joint movements using general motion detectors, or else global processes specialized for identifying posture changes over time). The neuroimaging measures employed in the present study provide evidence that autistic traits have variable impact on the two processing levels, which correspond to two different visual areas. Our finding that only STS activity (not MT) correlates with AQ highlights the importance of selecting tasks and stimuli to probe the global level of action processing when studying the impact of autism on biological motion perception.

In addition, our own recent paper (Van Boxtel et al., 2016) tested action adaptation ability in children with autism, using essentially the same paradigm. We found that children with autism show intact recognition performance for biological motion stimuli, but much weakened adaptation to actions. This convergence of findings supports the importance of the relationship between AQ scores and behavioral/neural adaptation found in the present paper. Although inferences from individual differences in the general population to people with ASC should be made with caution, we believe these results could help inform candidate neural mechanisms (in particular, right pSTS) underpinning dysfunction of social and perceptual processing within clinical populations at the extreme end of the Autistic spectrum.

Apart from neural aftereffects found in the right pSTS, we also found significant adaptation-induced changes in brain response to morphed actions within the left hMT+, but only when the test action was presented to the same location as the adaptor, confirming the retinal specificity of motion processing in this brain region. However, we did not find a significant correlation between neural aftereffects in hMT+ and perceptual aftereffects measured behaviorally, suggesting that these effects were likely due to lower-level adaptation to motion signals but did not contribute to final perceptual decision on certain attributes of actions. This result also suggest that testing for adaptation aftereffects in different retinal locations is an effective way to selectively probe higher-level neural populations with selectivity for more global stimulus properties such as faces (Kovács et al., 2008) and action category (van Boxtel and Lu, 2013a).

Many previous studies have examined repetition suppression effects using a measure called fMR-adaptation, a technique that has been used to determine the feature-tuning of neural populations at the sub-voxel level (Grill-Spector and Malach, 2001), and has helped to reveal the extent to which targeted neural populations contain action-specific representations for biological motion processing (Lestou et al., 2008; Grossman et al., 2010). In our study, the only area where we found significant fMR-adaptation originating from repetition suppression was in the right pSTS for repeated actions presented in the same location. While these results are consistent with previous fMR-adaptation results showing action-specific encoding in the right pSTS (Grossman et al., 2010), we did not find fMR-adaptation effects within bilateral hMT+, even for actions presented in the same location where presumably low-level, retinotopic motion adaptation should occur. We believe our null results may be due to factors related to experimental design, including the fact that we used actions with extremely similar low-level features (walking and running), whereas the study by Grossman et al. (2010) used a larger variety of actions (e.g., throwing, kicking, jumping jack) with very different low-level properties. Perhaps the local similarities among postures and motion features comprising our test stimuli reduced the power of our design for measuring repetition suppression effects. In other words, although our “different” stimuli did belong to a different action category, they may not have sufficiently differed to induce strong repetition suppression effects in the hemodynamic BOLD responses. This explanation is supported by another fMR-adaptation study investigating biological motion perception. In that study (Jastorff et al., 2009), actions were morphed between three different types of action, and fMR-adaptation was measured when two different morphs were presented in rapid succession. It was found that the pSTS did show fMR-adaptation to different morphs that were very similar, but hMT+ did not. Only after extensive training did the subjects begin to notice differences between the similar morphs, and only then did hMT+ start to show fMR-adaptation effects. This interpretation is further supported by research on face adaptation, in which a release from fMR-adaptation was found to occur only when the second face was perceived to be of a different identity than the first (Rotshtein et al., 2005).

Another plausible explanation for the lack of fMRI-adaptation effect is that the present study was designed specifically to measure brain activity associated with prolonged perceptual adaptation and hence utilized a topping-up adaptation paradigm to maintain a high level of adaptation strength throughout the block of trials. In contrast, studies designed to measure fMRI-adaptation will typically show two brief stimuli in rapid succession to measure repetition suppression. By design, our study aimed to maintain targeted neural populations in a highly adapted state throughout the scan, which could have reduced the degree of change in activity induced by stimulus repetition. On the other hand, this sustained level of adaptation could have helped to produce maximal changes in response to the ambiguous morphed action stimuli.

It is important to note that although repetition suppression effects were small, they also showed no pattern of correlation in

terms of individual differences with either behavioral performance or autistic traits. The fact that we repeatedly found a strong relationship between the change in neural response to morphed actions in right pSTS and these factors, coupled with the finding of a lack of relationship between behavior and fMR-adaptation, suggests that the physiological mechanisms that produce repetition suppression, which are currently under debate (Webster et al., 2005; Krekelberg et al., 2006; Caggiano et al., 2013), are likely distinct from those responsible for perceptual aftereffects. This conclusion is consistent with recent findings from a study of face adaptation (Kaiser et al., 2013), which also found evidence for a dissociation in these two types of adaptation. The extent to which these different mechanisms are engaged likely depends on the duration of the adaptation stimulus (Fang et al., 2007b; Kovács et al., 2008; Kaiser et al., 2013). Further studies will be required to fully characterize differences in the physiological mechanisms responsible for repetition suppression effects versus perceptual adaptation aftereffects in the human brain.

In addition to motion processing, form processing is also known to play a significant role in biological motion perception (Lange and Lappe, 2006; Thurman and Lu, 2014a). Theusner et al. (2011) found behavioral evidence to suggest two distinct types of action aftereffects – one that was linked more strongly to form processing, and the other linked to motion processing. In the current study, we measured perceptual aftereffects in different retinal locations to isolate local and global (e.g. non-retinotopic) adaptation effects. Based on prior brain studies, we had a specific hypothesis that the pSTS was the most likely brain region to show neural adaptation effects for actions at the global level. In contrast, we expected the motion sensitive area hMT+, which is involved in lower-level stages of motion processing, to serve as a logical comparison for pSTS to potentially differentiate between local and global levels of adaptation. Since this was the prime focus of the current study, we did not include a localizer for form-based regions involved in human body processing in ventral cortex, such as the extrastriate and fusiform body areas (Downing et al., 2001). Because we could not localize these brain regions, we are unable to determine whether form-based regions might have also contributed uniquely to perceptual aftereffects in the current study. Due to the overlap that is typically found in fMRI between hMT+ and the EBA region (Weiner and Grill-Spector, 2011), the possibility also remains that our measurements of hMT+ included some proportion of voxels with sensitivity to static human body postures. Examining the specific involvement of biological form processing areas remains an interesting and promising question to address in future work.

Taken as a whole, our results implicate the right pSTS as a primary neural substrate for directing perceptual decisions on biological motion by taking into consideration the temporal context of the action. On the other hand, although hMT+ is likely involved in the processing of dynamic information, it does not appear to directly contribute to perceptual aftereffects of biological motion, as evidenced by its location specificity and the overall lack of correlation to behavioral data. We further showed that neural aftereffects in the right hemisphere pSTS were strongly correlated with the degree of autistic traits in the typical population. The individual differences in action adaptation in the typically developing population may impact social interactions and understanding of others, and could help to explain, for example, the significant link between autistic traits and skills in science and mathematics – fields that generally demand much less social interaction (Baron-Cohen et al., 2001). This interpretation is predicated on the assumption that individuals will tend to participate in activities that engage their natural physical and cognitive strengths. Though speculative, we anticipate that future studies will help to further our understanding of the natural variance and complexities in human perception, cognition and social behavior, including variations along the autistic spectrum.

Acknowledgment

This work was supported by the UCLA Center for Autism Research and Training (CART pilot grant NIH/NICHD grant # P50-HK-055784 and National Center for Advancing Translational Sciences UCLA CTSI Grant UL1TR000124 to HL and MMM); National Science Foundation (BCS 1353391 to HL); and the James S. McDonnell Foundation (Scholar Award to MMM). We thank Junzhu Su who helped in data collection, and Hakwan Lau, Frank Pollick and Emily Grossman for helpful discussions and insightful suggestions.

References

- Baron-Cohen, S., Wheelwright, S., Skinner, R., Martin, J., Clubley, E., 2001. The autism-spectrum quotient (AQ): evidence from asperger syndrome/high-functioning autism, males and females, scientists and mathematicians. *J. Autism Dev. Disord.* 31, 5–17.
- Grill-Spector, K., Malach, R., 2001. fMR-adaptation: a tool for studying the functional properties of human cortical neurons. *Acta Psychol.* 107, 293–321.
- Allison, T., Puce, A., McCarthy, G., 2000. Social perception from visual cues: role of the STS region. *Trends Cogn. Sci.* 4, 267–278.
- Blake, R., Shiffrar, M., 2007. Perception of human motion. *Annu. Rev. Psychol.* 58, 47–73.
- Boynton, G.M., Engel, S.A., Glover, G.H., Heeger, D.J., 1996. Linear systems analysis of functional magnetic resonance imaging in human V1. *J. Neurosci.* 16, 4207–4221.
- Caggiano, V., Pomper, J.K., Fleischer, F., Fogassi, L., Giese, M., Thier, P., 2013. Mirror neurons in monkey area F5 do not adapt to the observation of repeated actions. *Nat. Commun.* 4, 1433.
- Castelli, F., Happé, F., Frith, U., Frith, C., 2000. Movement and mind: a functional imaging study of perception and interpretation of complex intentional movement patterns. *NeuroImage* 12, 314–325.
- Clifford, C.W.G., Webster, M.A., Stanley, G.B., Stocker, A.A., Kohn, A., Sharpee TO, Schwartz, O., 2007. Visual adaptation: neural, psychological and computational aspects. *Vis. Res.* 47, 3125–3131.
- Chang, C.C., Lin, C.J., 2011. LIBSVM: a library for support vector machines. *ACM Trans. Intell. Syst. Technol.* 2, 27.
- Cusack, J.P., Williams, J.H., Neri, P., 2015. Action perception is intact in autism spectrum disorder. *J. Neurosci.* 35, 1849–1857.
- Dale, A.M., Buckner, R.L., 1997. Selective averaging of rapidly presented individual trials using fMRI. *Hum. Brain Mapp.* 5, 329–340.
- Dale, A.M., 1999. Optimal experimental design for event-related fMRI. *Hum. Brain Mapp.* 8, 109–114.
- Downing, P.E., Jiang, Y., Shuman, M., Kanwisher, N., 2001. A cortical area selective for visual processing of the human body. *Science* 293, 2470–2473.
- Fang, F., Ijichi, K., He, S., 2007a. Transfer of the face viewpoint aftereffect from adaptation to different and inverted faces. *J. Vis.* 7, 1–9.
- Fang, F., Murray, S.O., He, S., 2007b. Duration-dependent fMRI adaptation and distributed viewer-centered face representation in human visual cortex. *Cereb. Cortex* 17, 1402–1411.
- Freitag, C.M., Konrad, C., Häberlein, M., Kleser, C., von Gontard, A., Reith, W., Troje, N.F., Krick, C., 2008. Perception of biological motion in autism spectrum disorders. *Neuropsychologia* 46, 1480–1494.
- Gallagher, H.L., Happé, F., Brunswick, N., Fletcher, P.C., Frith, U., Frith, C.D., 2000. Reading the mind in cartoons and stories: an fMRI study of “theory of mind” in verbal and nonverbal tasks. *Neuropsychologia* 38, 11–21.
- Giese, M.A., Poggio, T., 2000. Morphable models for the analysis and synthesis of complex motion patterns. *Int. J. Comput. Vis.* 38, 59–73.
- Grossman, E.D., Blake, R., 2002. Brain areas active during visual perception of biological motion. *Neuron* 35, 1167–1175.
- Grossman, E., Donnelly, M., Price, R., Pickens, D., Morgan, V., Neighbor, G., Blake, R., 2000. Brain areas involved in perception of biological motion. *J. Cogn. Neurosci.* 12, 711–720.
- Grossman, E.D., Jardine, N.L., Pyles, J., 2010. fMR-adaptation reveals invariant coding of biological motion on the human STS. *Front. Hum. Neurosci.* 4, 15.
- Herrington, J.D., Baron-Cohen, S., Wheelwright, S.J., Singh, K.D., Bullmore, E.T., Brammer, M., Williams, S.C.R., 2007. The role of MT+/V5 during biological motion perception in Asperger syndrome: an fMRI study. *Res. Autism. Spectr. Disord.* 1, 14–27.
- Huk, A.C., Dougherty, R.F., Heeger, D.J., 2002. Retinotopy and functional subdivision of human areas MT and MST. *J. Neurosci.* 22, 7195–7205.
- Jackson, S., Blake, R., 2010. Neural integration of information specifying human structure from form, motion, and depth. *J. Neurosci.* 30, 838–848.
- Jastorff, J., Kourtzi, Z., Giese, M.A., 2009. Visual learning shapes the processing of complex movement stimuli in the human brain. *J. Neurosci.* 29, 14026–14038.
- Jenkinson, M., Smith, S., 2001. A global optimisation method for robust affine registration of brain images. *Med. Image Anal.* 5, 143–156.
- Jenkinson, M., Bannister, P., Brady, M., Smith, S., 2002. Improved optimization for the robust and accurate linear registration and motion correction of brain images. *NeuroImage* 17, 825–841.
- Johansson, G., 1973. Visual perception of biological motion and a model for its analysis. *Percept. Psychophys.* 14, 201–211.
- Kaiser, M.D., Pelphrey, K.A., 2012. Disrupted action perception in autism: behavioral evidence, neuroendophenotypes, and diagnostic utility. *Dev. Cogn. Neurosci.* 2, 25–35.
- Kaiser, D., Walther, C., Schweinberger, S.R., Kovács, G., 2013. Dissociating the neural bases of repetition-priming and adaptation in the human brain for faces. *J. Neurophysiol.* 110, 2727–2738.
- Klin, A., Lin, D.J., Gorrindo, P., Ramsay, G., Jones, W., 2009. Two-year-olds with autism orient to non-social contingencies rather than biological motion. *Nature* 459, 257–261.
- Kourtzi, Z., Kanwisher, N., 2000. Cortical regions involved in perceiving object shape. *J. Neurosci.* 20, 3310–3318.
- Kourtzi, Z., Tolia, A.S., Altmann, C.F., Augath, M., Logothetis, N.K., 2003. Integration of local features into global shapes: monkey and human fMRI studies. *Neuron* 37, 333–346.
- Kovács, G., Cziraki, C., Vidnyánszky, Z., Schweinberger, S.R., Greenlee, M.W., 2008. Position-specific and position-invariant face aftereffects reflect the adaptation of different cortical areas. *NeuroImage* 43, 156–164.
- Krekelberg, B., Boynton, G.M., van Wezel, R.J.A., 2006. Adaptation: from single cells to BOLD signals. *Trends Neurosci.* 29, 250–256.
- Kriegeskorte, N., Simmons, W.K., Bellgowan, P.S.F., Baker, C.I., 2009. Circular analysis in systems neuroscience: the dangers of double dipping. *Nat. Neurosci.* 12, 535–540.
- Lange, J., Lappe, M., 2006. A model of biological motion perception from configural form cues. *J. Neurosci.* 26, 2894–2906.
- Lestou, V., Pollick, F.E., Kourtzi, Z., 2008. Neural substrates for action understanding at different description levels in the human brain. *J. Cogn. Neurosci.* 20, 324–341.
- McAleer, P., Kay, J.W., Pollick, F.E., Rutherford, M.D., 2011. Intention perception in high functioning people with Autism Spectrum Disorders using animacy displays derived from human actions. *J. Autism Dev. Disord.* 41, 1053–1063.
- McKay, L.S., Simmons, D.R., McAleer, P., Marjoram, D., Piggot, J., Pollick, F.E., 2012. Do distinct atypical cortical networks process biological motion information in adults with Autism Spectrum Disorders? *NeuroImage* 59, 1524–1533.
- Michels, L., Kleiser, R., De Lussanet, M.H.E., Seitz, R.J., Lappe, M., 2009. Brain activity for peripheral biological motion in the posterior superior temporal gyrus and the fusiform gyrus: dependence on visual hemifield and view orientation. *NeuroImage* 45, 151–159.
- Mumford, J.A., Turner, B.O., Ashby, F.G., Poldrack, R.A., 2012. Deconvolving BOLD activation in event-related designs for multivoxel pattern classification analyses. *NeuroImage* 59, 2636–2643.
- Murphy, P., Brady, N., Fitzgerald, M., Troje, N.F., 2009. No evidence for impaired perception of biological motion in adults with autistic spectrum disorders. *Neuropsychologia* 47, 3225–3235.
- Narumoto, J., Okada, T., Sadato, N., Fukui, K., Yonekura, Y., 2001. Attention to emotion modulates fMRI activity in human right superior temporal sulcus. *Cogn. Brain Res.* 12, 225–231.
- Nili, H., Wingfield, C., Walther, A., Su, L., Marslen-Wilson, W., Kriegeskorte, N., 2014. A toolbox for representational similarity analysis. *PLoS Comput. Biol.* 10, e1003553.
- Pavlova, M., 2012. Biological motion processing as a hallmark of social cognition. *Cereb. Cortex* 22, 981–995.
- Pellicano, E., Jeffery, L., Burr, D., Rhodes, G., 2007. Abnormal adaptive face-coding mechanisms in children with autism spectrum disorder. *Curr. Biol.* 17, 1508–1512.
- Pelphrey, K.A., Morris, J.P., McCarthy, G., 2004. Grasping the intentions of others: the perceived intentionality of an action influences activity in the superior temporal sulcus during social perception. *J. Cogn. Neurosci.* 16, 1706–1716.
- Pelphrey, K.A., Morris, J.P., Michelich, C.R., Allison, T., McCarthy, G., 2005. Functional anatomy of biological motion perception in posterior temporal cortex: an fMRI study of eye, mouth and hand movements. *Cereb. Cortex* 15, 1866–1876.
- Peuskens, H., Vanrie, J., Verfaillie, K., Orban, G.A., 2005. Specificity of regions processing biological motion. *Eur. J. Neurosci.* 21, 2864–2875.
- Preacher, K.J., Rucker, D.D., MacCallum, R.C., Nicewander, W.A., 2005. Use of the extreme groups approach: a critical reexamination and new recommendations. *Psych Meth* 10, 178.
- Prins, N., FAA, K., 2009. Palamedes: Matlab routines for analyzing psychophysical data. (Available at:) <http://www.palamedestoolbox.org>.
- Pyles, J.A., Garcia, J.O., Hoffman, D.D., Grossman, E.D., 2007. Visual perception and neural correlates of novel “biological motion. *Vis. Res.* 47, 2786–2797.
- Rissman, J., Gazzaley, A., D’Esposito, M., 2004. Measuring functional connectivity during distinct stages of a cognitive task. *NeuroImage* 23, 752–763.
- Rotshtein, P., Henson, R.N.A., Driver, J., Dolan, R.J., 2005. Morphing Marilyn into Maggie dissociates physical and identity face representations in the brain. *Nat. Neurosci.* 8, 107–113.
- Saygin, A.P., Cook, J., Blakemore, S.J., 2010. Unaffected perceptual thresholds for biological and non-biological form-from-motion perception in autism spectrum conditions. *PLoS One* 5.
- Saygin, A.P., 2007. Superior temporal and premotor brain areas necessary for biological motion perception. *Brain* 130, 2452–2461.
- Serences, J.T., 2004. A comparison of methods for characterizing the event-related BOLD timeseries in rapid fMRI. *NeuroImage* 21, 1690–1700.
- Smith, S.M., Jenkinson, M., Woolrich, M.W., Beckmann, C.F., Behrens, T.E.J., Johansen-Berg, H., Bannister, P.R., De Luca, M., Drobnjak, I., Flitney, D.E., Niazy, R.K., Saunders, J., Vickers, J., Zhang, Y., De Stefano, N., Brady, J.M., Matthews, P.M., 2004. Advances in functional and structural MR image analysis and implementation as FSL. *NeuroImage* 23, S208–S219.
- Theusner, S., De Lussanet, M.H.E., Lappe, M., 2011. Adaptation to biological motion leads to a motion and a form aftereffect. *Atten. Percept. Psychophys.* 73, 1843–1855.
- Thompson, J.C., Baccus, W., 2011. Form and motion make independent contributions to the response to biological motion in occipitotemporal cortex. *NeuroImage* 59, 625–634.
- Thurman, S.M., Lu, H., 2013a. Complex interactions between spatial, orientation, and motion cues for biological motion perception across visual space. *J. Vis.* 13, 1–18.

- Thurman, S.M., Lu, H., 2013b. Physical and biological constraints govern perceived animacy of scrambled human forms. *Psychol. Sci.* 24, 1133–1141.
- Thurman, S.M., Lu, H., 2014a. Bayesian integration of position and orientation cues in perception of biological and non-biological forms. *Front. Hum. Neurosci.* 8, 91.
- Thurman, S.M., Lu, H., 2014b. Perception of social interactions for spatially scrambled biological motion. *PLoS ONE* 9, e112539.
- Troje, N.F., Sadr, J., Geyer, H., Nakayama, K., 2006. Adaptation aftereffects in the perception of gender from biological motion. *J. Vis.* 6, 850–857.
- Van Boxtel, J.J.A., Lu, H., 2012. Signature movements lead to efficient search for threatening actions. *PLoS ONE* 7, e37085.
- Van Boxtel, J.J.A., Lu, H., 2013a. Impaired global, and compensatory local, biological motion processing in people with high levels of autistic traits. *Front. Psychol.* 4, 209.
- Van Boxtel, J.J.A., Lu, H., 2013b. A biological motion toolbox for reading, displaying, and manipulating motion capture data in research settings. *J. Vis.* 13, 1–16.
- Van Boxtel, J.J., Dapretto, M., Lu, H., 2016. Intact recognition, but attenuated adaptation, for biological motion in youth with autism spectrum disorder. *Autism Res.* <http://dx.doi.org/10.1002/aur.1595> (Early view of online version).
- Webster MA, Werner J, Field D. 2005. Adaptation and the phenomenology of perception. In: *Fitting the Mind to the World: Adaptation and Aftereffects in High-Level Vision, Advances in Visual Cognition Series.* (Clifford CW, Rhodes, GL, eds), pp 241–277. New York: Oxford UP.
- Webster, M.A., 2011. Adaptation and visual coding. *J. Vis.* 11.
- Weiner, K.S., Grill-Spector, K., 2011. Not one extrastriate body area: using anatomical landmarks, hMT+, and visual field maps to parcellate limb-selective activations in human lateral occipitotemporal cortex. *NeuroImage* 56, 2183–2199.
- Weiner, K.S., Sayres, R., Vinberg, J., Grill-Spector, K., 2010. fMRI-adaptation and category selectivity in human ventral temporal cortex: regional differences across time scales. *J. Neurophysiol.* 103, 3349–3365.
- Zhang, X., Qiu, J., Zhang, Y., Han, S., Fang, F., 2014. Misbinding of color and motion in human visual cortex. *Curr. Biol.* 24, 1354–1360.